Volume 27

Published on 05 February 2015 on http://pubs.rsc.org | doi:10.1039/9781782622697-FP001
Downloaded on .

View Online

Published on 05 February 2015 on http://pubs.rsc.org | doi:10.1039/9781782622697-FP001
Downloaded on .

View Online

A Specialist Periodical Report

Catalysis

Volume 27

A Review of Recent Literature

Editors
James J. Spivey, *Louisiana State University, USA*
Yi-Fan Han, *East China University of Science and Technology, Shanghai, China*
K. M. Dooley, *Louisiana State University, USA*

Authors
Javier Barrientos, *KTH - Royal Institute of Technology, Sweden*
Magali Boutonnet, *KTH - Royal Institute of Technology, Sweden*
Angelika Brückner, *Leibniz-Institut für Katalyse e. V. an der Universität Rostock, Germany*
Zhuo Cheng, *Washington University, USA*
Vadim V. Guliants, *University of Cincinnati, USA*
Dirk Hollmann, *Leibniz-Institut für Katalyse e. V. an der Universität Rostock, Germany*
Sven Järås, *KTH - Royal Institute of Technology, Sweden*
Eunmin Lee, *Washington University, USA*
Hexing Li, *Shanghai Normal University, China*
Hui Li, *Shanghai Normal University, China*
Cynthia S. Lo, *Washington University, USA*
Luis López, *KTH - Royal Institute of Technology, Sweden and Universidad Mayor de San Andrés, Boliva*
Fátima Pardo, *KTH - Royal Institute of Technology, Sweden and Universidad Mayor de San Andrés, Boliva*
Thomas Risse, *Freie Universität Berlin, Germany*
Rodrigo Suárez París, *KTH - Royal Institute of Technology, Sweden*
Hongqi Sun, *Curtin University, Australia*
Shaobin Wang, *Curtin University, Australia*
Wei Wei, *Shanghai Normal University, China*
Yu Zhao, *Shanghai Normal University, China*

Published on 05 February 2015 on http://pubs.rsc.org | doi:10.1039/9781782622697-FP001
Downloaded on .

ROYAL SOCIETY OF CHEMISTRY

THE QUEEN'S AWARDS FOR ENTERPRISE: INTERNATIONAL TRADE 2013

View Online

Published on 05 February 2015 on http://pubs.rsc.org | doi:10.1039/9781782622697-FP001
Downloaded on .

ISBN: 978-1-78262-054-9
eISBN: 978-1-78262-269-7
DOI: 10.1039/9781782622697
ISSN: 0140-0568

A catalogue record for this book is available from the British Library

© The Royal Society of Chemistry 2015

All rights reserved

Apart from any fair dealing for the purpose of research or private study for non-commercial purposes, or criticism or review, as permitted under the terms of the UK Copyright, Designs and Patents Act, 1988 and the Copyright and Related Rights Regulations 2003, this publication may not be reproduced, stored or transmitted, in any form or by any means, without the prior permission in writing of The Royal Society of Chemistry, or in the case of reprographic reproduction only in accordance with the terms of the licences issued by the Copyright Licensing Agency in the UK, or in accordance with the terms of the licences issued by the appropriate Reproduction Rights Organization outside the UK. Enquiries concerning reproduction outside the terms stated here should be sent to The Royal Society of Chemistry at the address printed on this page.

Published by The Royal Society of Chemistry,
Thomas Graham House, Science Park, Milton Road,
Cambridge CB4 0WF, UK

Registered Charity Number 207890

For further information see our web site at www.rsc.org

Preface

DOI: 10.1039/9781782622697-FP005

Published on 05 February 2015 on http://pubs.rsc.org | doi:10.1039/9781782622697-FP005
Downloaded on .

Chapter 1: Preparation and catalytic applications of amorphous alloys
In this chapter, preparation and catalytic applications of amorphous alloys is reviewed by Hui Li, Wei Wei, Yu Zhao, and Hexing Li from Shanghai Normal University, Shanghai, China. Amorphous alloys are one of the most important catalytic materials and considered as a new generation of metallic catalysts. Mastery over the composition and/or morphology of amorphous alloy enables control of its properties and enhancement of its applications as catalyst. The aim of this chapter is to present the recent developments in the design- and fabrication of amorphous alloys through a chemical reduction method with an emphasis on composition- and morphology control. The examples discussed in this review highlight the need to design and synthesis of amorphous alloy with controllable composition or morphology in order to promote catalytic performances. Perhaps more importantly, they also are of value for researchers in the area of heterogeneous catalysis to develop highly-efficient metallic catalysts.

Chapter 2: *In situ* electron paramagnetic resonance (EPR) – a unique tool for analysing structure and reaction behaviour of paramagnetic sites in model and real catalysts
In the next review, *In situ* electron paramagnetic resonance is reviewed by Thomas Risse, Dirk Hollmann and Angelika Brückner from University of Rostock, Rostock, Mecklenburg-Vorpommern, Germany. The majority of catalytic reactions involves reduction and/or reoxidation steps in which electrons are transferred between catalysts and substrates. EPR spectroscopy can sensitively probe the local environment of paramagnetic catalytic sites as well as their behavior in catalytic redox processes since it can be applied under a wide range of conditions. After a short summary of the most important application examples of *in situ* EPR in redox catalysis, the main features of EPR spectra such g and A matrices and approaches of their evaluation are presented using model systems that contain Au atoms deposited on MgO single crystal surfaces. To illustrate the versatility of *in situ* EPR for deriving structure–reactivity relationships in catalysis, two application examples are presented in more detail: (1) Analysis of heterogeneous supported VO_x/TiO_2 catalysts during oxidative dehydrogenation of propane in the gas phase and (2) Study of photocatalytic water splitting over a homogeneous catalytic system comprising an iridium photosensitizer complex and an iron carbonyl catalyst.

Chapter 3: Present and future prospects in heterogeneous catalysts for C_1 chemistry
Eunmin Lee, Zhuo Cheng, and Cynthia S. Lo (Washington University, St. Louis, USA) examine the recent research and development in catalysis of C_1 reactants, including significant reactions involving CO_2 and CH_4. The conversion of these thermodynamically stable reactants into higher

© The Royal Society of Chemistry 2015

Published on 05 February 2015 on http://pubs.rsc.org | doi:10.1039/9781782622697-FP005
Downloaded on .

volume and higher value products is a key challenge. There is particular interest in converting these C_1 reactants into higher carbon-number products, such as higher oxygenates and liquid fuels. Studies to examine various bond-breaking and bond-forming reactions are in the heart of catalytic research. Examples of recent advances include synthesis and catalytic understanding of reactions on metal nanoparticles, redox-active metal oxide supports, zeolite catalysts, and the use of ionic liquids. These are the result of characterization tools that we anticipate will drive C_1 development over the next decade.

Chapter 4: Catalytic oxidation of organic pollutants in aqueous solution using sulfate radicals

An area of increasing importance in catalysis is its application to water purification. In this review, Hongqi Sun and Shaobin Wang of Curtin University, Australia, review recent progress in advanced oxidation processes as applied to organic contaminants in aqueous media. The focus is on the interaction of catalyst with persulfate and peroxymonosulfate ions. However, purely photolytic processes, and those which are light-assisted, are considered as well. Keys to more effective utilization of the sulfates are explored.

Chapter 5: Catalytic conversion of biomass-derived synthesis gas to fuels

This topic is timely, but its breadth requires a substantial joint effort, here from groups at both the Royal Institute of Technology (KTH) in Sweden and Universidad Mayor de San Andrés in Bolivia. The effort is led by Rodrigo Suárez París of KTH. The authors first introduce the subject by exploring the nature (compositions, physical properties) of typical biomassgasifier effluents, then consider in turn the Fischer-Tropsch, substitute natural gas, ethanol/mixed alcohols, and methanol/dimethyl ether upgrading processes. They also explore further catalytic upgrades to certain Fischer-Tropsch products. In each case, they cover not only the descriptive catalysis, but also consider mechanism, thermodynaics, and process details.

Chapter 6: Theoretical studies of selective propane oxidation and ammoxidation over vanadium-based multi-metal oxides

One of the most studied catalytic processes is here re-examined by Vadim Guliants of the University of Cincinnati. But in the present review the focus is on recent insights provided by theoretical studies, in particular density functional theory simulations of the surface of the important Mo–V–Te–Nb–O M1 phase catalyst. These studies have led to new mechanistic insights into the initial propane activation steps. Recent studies are now beginning to shed light on the entire multielectron reaction pathway for propane ammoxidation on multicomponent bulk metal oxides, using a combination of CI-NEB and dimer methods. For the M1 surface, it was found that V^{5+}=O is the preferred surface site for all three H abstraction steps, and that H abstraction from propane is the rate-determining step for propane ammoxidation.

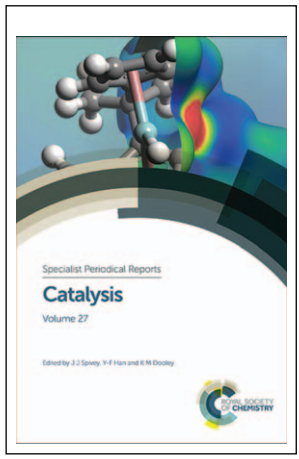

Cover

Image provided courtesy of computational science company Accelrys (www.accelrys.com). An electron density isosurface mapped with the electrostatic potential for an organometallic molecule. This shows the charge distribution across the surface of the molecule with the red area showing the positive charge associated with the central metal atom. Research carried out using Accelrys Materials Studios®.

Published on 05 February 2015 on http://pubs.rsc.org | doi:10.1039/9781782622697-FP007
Downloaded on .

© The Royal Society of Chemistry 2015

View Online

Published on 05 February 2015 on http://pubs.rsc.org | doi:10.1039/9781782622697-FP007
Downloaded on .

In situ electron paramagnetic resonance (EPR) – a unique tool for analysing structure and reaction behaviour of paramagnetic sites in model and real catalysts

Thomas Risse,[a] Dirk Hollmann[b] and Angelika Brückner*[b]

DOI: 10.1039/9781782622697-00001

Published on 05 February 2015 on http://pubs.rsc.org | doi:10.1039/9781782622697-00001
Downloaded on .

The majority of catalytic reactions involves reduction and/or reoxidation steps in which electrons are transferred between catalysts and substrates. EPR spectroscopy can sensitively probe the local environment of paramagnetic catalytic sites as well as their behavior in catalytic redox processes since it can be applied under a wide range of conditions. After a short summary of the most important application examples of *in situ* EPR in redox catalysis, the main features of EPR spectra such *g* and *A* matrices and approaches of their evaluation are presented using model systems that contain Au atoms deposited on MgO single crystal surfaces. To illustrate the versatility of *in situ* EPR for deriving structure–reactivity relationships in catalysis, two application examples are presented in more detail: (1) Analysis of heterogeneous supported VO_x/TiO_2 catalysts during oxidative dehydrogenation of propane in the gas phase and (2) Study of photocatalytic water splitting over a homogeneous catalytic system comprising an iridium photosensitizer complex and an iron carbonyl catalyst.

1 Introduction

EPR spectroscopy has been used to characterize catalysts since very early on, because of its ability to provide detailed information on paramagnetic species such as their geometric and electronic structure or their chemical environment. In terms of the systems being investigated, EPR covers a wide range of applications from heterogeneous, *via* homogeneous catalysts all the way to enzymatic systems. Paramagnetic species in catalytic systems range from sites considered crucial for catalytic turnover, such as transition metal ions, to paramagnetic reaction intermediates. Analyzing their behavior *in situ*, *i.e.* under conditions as close as possible to those of a catalytic reaction, can be most helpful for deriving structure–reactivity relationships and reaction mechanisms. Nevertheless, applications of *in situ* EPR spectroscopy for monitoring catalytic reactions are not as numerous compared to other common methods such as vibrational spectroscopy or X-ray techniques, due to the fact that it is restricted to systems containing unpaired electrons. However, for catalytic redox processes in which electrons are transferred between catalyst and

[a]*Institut für Chemie und Biochemie, Freie Universität Berlin, Takustr. 3, 14195 Berlin, Germany*
[b]*Leibniz-Institut für Katalyse e. V. an der Universität Rostock, Albert-Einstein-Str. 29a, 18059 Rostock, Germany. E-mail: angelika.brueckner@catalysis.de*

© The Royal Society of Chemistry 2015

Published on 05 February 2015 on http://pubs.rsc.org | doi:10.1039/9781782622697-00001
Downloaded on .

reactants, *in situ* EPR (or *operando* EPR, as it is called when together with the EPR spectrum catalytic conversion/selectivity data are measured) is a unique tool, since it can visualize this electron transfer directly as long as paramagnetic species are involved. This has been illustrated in the past for a variety of hydrocarbon conversion reactions. Thus, mixed oxide and oxynitride bulk phases such as vanadium–phosphorus oxides,[1] vanadium–molybdenum oxides,[2] mixed VTiSbSi oxides,[3] VAlON and VZrON oxynitrides[4] or heteropolyacids of defined structure[5] have been used for selective oxidation of alkanes and aromatics. Such reactions have also been monitored by *in situ* EPR over supported vanadia and bismuth molybdate catalysts[1] while supported chromia[1] and nickel catalysts[6,7] were studied during non-oxidative aromatization of alkanes as well as during interaction with butenes. Another important class of heterogeneous catalytic systems analysed by *in situ* EPR comprises zeolites containing transition metal ions either incorporated in the framework or located in pore positions. Many of such catalysts have been used to remove nitrogen oxides (NO_x) from exhaust gases. Relevant examples comprise the use of Co–BEA[8] and Fe–ZSM-5[9] for selective catalytic reduction of NO_x, but also Cu–ZSM-5 has been widely used for the same purpose by Kucherov *et al.*, whose work has been reviewed in ref. 1. The interaction of benzene with oxygen has been recently studied on the same type of catalysts to understand the gas-phase oxidation of benzene to phenol.[10] For a more comprehensive selection of application examples for *in situ* EPR in heterogeneous catalysis the reader is referred to a number of reviews.[1,2,11–13] Surprisingly, the use of *in situ* EPR spectroscopy for elucidating structure–reactivity relationships in homogeneous redox catalysis is even more limited than in heterogeneous catalysis.

In EPR spectroscopy the sample is placed in an external magnetic field to lift the degeneracy of the electron spin states and microwave radiation is used to induce magnetic dipole transitions between these states. Historically, most of the information has been obtained using continuous wave EPR spectroscopy operating at a microwave frequency of $\approx$10 GHz in the so-called X-band. Spectrometers of this kind are still by far the most abundant ones, however, the last decades have seen a significant diversification of experimental capabilities, namely, the commercial availability of spectrometers operating at different microwave frequencies as well as pulse spectrometers, which enables the use of these techniques also outside of laboratories dedicated to instrumental developments in EPR spectroscopy.[14,15]

The aim of this chapter is to acquaint the reader with the basic principles and application opportunities of *in situ* EPR in redox catalysis. The introductory part starts with a presentation of instrumental aspects and experimental procedures (Section 2), followed by a discussion of the most important parameters, the g and A matrix components, that can be derived from EPR spectra (Section 3). Here we will focus on the examples of Au atoms and $O_2^{\bullet-}$ radicals deposited on a MgO(001) surface, which both represent the simplest case of paramagnetic species with a single unpaired electron and a spin of $S = 1/2$. We will restrict ourselves to the

Published on 05 February 2015 on http://pubs.rsc.org | doi:10.1039/9781782622697-00001
Downloaded on .

analysis of cw EPR spectra being still the most common ones and typically the initial step in an EPR spectroscopic investigation. This discussion will be amended by only very few examples of pulse EPR techniques (Section 4), which provide valuable additional information on hyperfine interactions in paramagnetic species that can reflect peculiarities of their environment with much higher resolution than cw EPR.

In the application oriented part of this chapter (Section 5), we present two case studies, which illustrate the potential of *in situ* EPR for deriving structure–reactivity relationships in both heterogeneous and homogeneous catalytic redox processes, whereby special benefits arising from the coupling of *in situ* EPR with other techniques are explicitly pointed out. The first example is dedicated to a supported VO_x/TiO_2 catalyst. Such catalysts are of paramount importance for a variety of heterogeneous catalytic redox processes. Thus, V_2O_5/TiO_2 modified by WO_3 (also known as EUROCAT oxide) is an industrial catalyst for selective catalytic reduction of NO_x in power plant exhaust gases, which has been studied in a round robin test by many European catalysis laboratories.[16] Besides, there is a multitude of papers, among them those containing *operando* EPR studies[17–19] in which the use of supported V_2O_5/TiO_2 catalysts is described for a variety of catalytic oxidation reactions. In the first case study, the influence of surface sulfates on the structure of VO_x species dispersed on the surface of titania[20] and their catalytic behaviour in the oxidative dehydrogenation of propane to propene is analyzed by *operando* EPR coupled with UV-vis diffuse reflectance and laser-Raman spectroscopy.[18] The second case study illustrates the special benefits of *in situ* EPR, supported by vibrational spectroscopy, for elucidating the mechanism of photocatalytic water reduction in a homogeneous catalytic system. A similar approach has been used very recently to unravel different wavelength dependent electron transfer mechanisms in plasmonic Au/TiO_2 water splitting catalysts.[21] The selection of these case studies was done with the aim to highlight the versatility of *in situ* EPR spectroscopy for a wide variety of reaction conditions, as long as paramagnetic species are involved.

2 Basic experimental considerations

Prior to a discussion of the appearance of EPR spectra it is appropriate to spend some time on experimental considerations. Herein, the discussion will be restricted to cw spectroscopy. With respect to pulse spectroscopy the interested reader is referred to the literature (*e.g.* ref. 22). EPR spectroscopy probes the properties of paramagnetic species by means of magnetic dipole transitions. Because of the small oscillator strength of such magnetic dipole transitions resonators are widely used in EPR spectroscopy to enhance the magnetic field strength at the sample. The properties of the resonator, which can be characterized by quantities such as the quality factor, filling factor or conversion efficiency, crucially determine the performance of the experiment. The use of resonators typically implies that monochromatic radiation has to be used, which

Published on 05 February 2015 on http://pubs.rsc.org | doi:10.1039/9781782622697-00001
Downloaded on .

forms a standing wave pattern inside the resonator. Additionally, the resonator structures lead to a separation of the magnetic from the electric field component helping to reduce undesired electric dipole excitations. The reader is referred to the literature for a more comprehensive discussion.[23]

The EPR spectrum is obtained by sweeping the external magnetic field. Despite the fact that resonator structures are used, the amount of absorbed radiation is still very small. To improve the signal-to-noise ratio of the spectrum, cw-EPR spectrometers use a lock-in detection scheme. To this end, the external magnetic field is modulated with a known frequency and phase, which allows phase sensitive detection of the corresponding Fourier component of the detector signal. While this sounds like a pure technicality it has the important consequence that cw-EPR spectra are recorded as the first derivative of the absorption spectrum, more precisely: the first derivative of the imaginary part of the complex high frequency susceptibility by the field ($d\chi''/dB$) as a function of the magnetic field. The number of spins may be determined from such a spectrum by double integration. This has to be done with care to avoid artefacts, *e.g.* due to imperfections of the baseline. Because of the direct relation of the EPR signal with the susceptibility of paramagnetic samples, the intensity of the EPR signal should obey Curie's law, which predicts an inverse proportionality of the magnetic susceptibility and, hence, the EPR signal intensity with temperature. A simple and often used test for Curie behavior is to plot the EPR signal intensity multiplied by the sample temperature ($I \times T$) as a function of the temperature. For a paramagnetic sample with a constant number of spins, this product should be constant and deviations from this may be discussed as changes in the amount of paramagnetic species detected by the spectroscopy at different temperatures. For catalytic systems containing species, which may adopt paramagnetic as well as diamagnetic states, such as transition metal centres, temperature dependent measurements of the EPR signal intensity are a rather simple test to monitor the amount of paramagnetic species for different conditions. It is important to note that it is the signal area of an individual species and not simply the peak-to-peak amplitude of a line or the integral intensity of the entire spectrum, which needs to be considered. The latter two quantities may be used under appropriate conditions, too. The analysis of the temperature dependent intensity as outlined above also assumes that the experimental conditions will not induce additional changes in the measured spectrum. To this end, saturation effects may be one source of error, because relaxation times are a function of temperature. Unfavourable relaxation properties may also be responsible for the difficulty to observe paramagnetic species at certain temperatures. It is well known that not all paramagnetic species can be observed by EPR at all temperatures. Prominent examples are certain transition metal ions such as Co^{2+} or Ni^{2+}, which typically require very low temperature to be observed. The relaxation behaviour of paramagnetic centres is one of the important issues to be considered in detail when one tries to apply EPR spectroscopy as an *operando* technique in catalysis. Despite the importance of relaxation phenomena for EPR,

a more detailed discussion goes beyond the scope of this introductory part and the interested reader is referred to the literature on this topic.[24–28]

3 Cw EPR spectroscopy of spin 1/2 systems

3.1 Paramagnetic species on solid surfaces

The key step in the interpretation of EPR spectra is to identify the various underlying physical effects by analysing appropriate EPR spectra. In order to get acquainted with the language typically used in EPR spectroscopy within this introductory chapter we will restrict the discussion to systems with a spin doublet ground state. Placing such a doublet state in a magnetic field leads to a splitting of the two spin states $S = \pm 1/2$ according to Zeeman interaction, which gives rise to a linear dependence of the energy difference between the spin states from the magnetic field. This shall be exemplified using Au atoms, which are characterized by an unpaired electron in the 6s orbital leading to a ^{2}S ground state. In the particular example presented here Au atoms are deposited on a single crystalline MgO(001) surface at 30 K to prevent diffusion of the atoms, which would lead to the formation of nanoparticles. The experiments were done under ultrahigh vacuum conditions ($p < 1 \times 10^{-10}$ mbar) to ensure that the results are not perturbed by the interaction with molecules from the gas phase. For the magnetic field being oriented parallel to the surface, Au atoms on MgO(001) show an EPR spectrum as presented in Fig. 1a.[29]

In contrast to the simple consideration based on the Zeeman interaction of the doublet ground state, it does not show a single line, but four

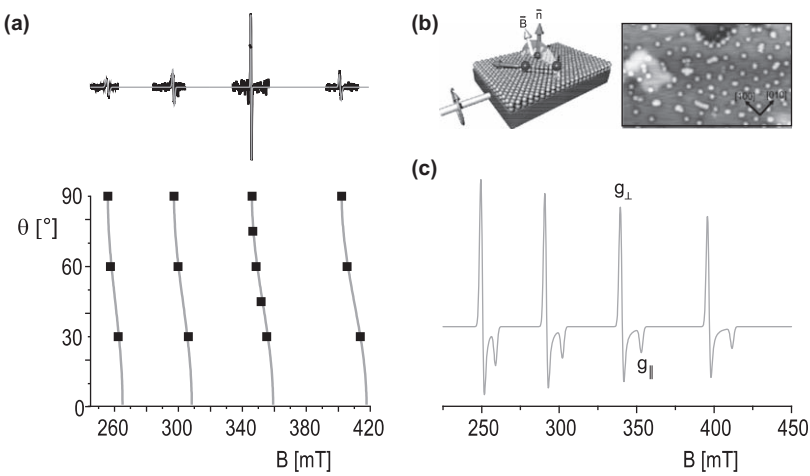

Fig. 1 (a) Top: EPR spectrum of 0.0025 ML Au on 20 ML MgO(001)/Mo(001) ($T = 30°$ K), $B_{\parallel}$ to surface (black trace); grey trace: simulation of the spectrum using the magnetic parameters given in Table 1 (for details see also text); bottom: resonance position as a function of the angle between the external magnetic field and the surface normal; black dots – experimental points; grey traces – simulation. (b) Left: schematic sketch of the experimental geometry, right: low temperature STM of Au atoms on an 8 ML MgO(001) film. (c) Expected EPR spectrum for Au atoms on MgO powder (properties as on the (001) surface).

Published on 05 February 2015 on http://pubs.rsc.org | doi:10.1039/9781782622697-00001
Downloaded on .

Published on 05 February 2015 on http://pubs.rsc.org | doi:10.1039/9781782622697-00001
Downloaded on .

non-equidistant lines of considerably different amplitude. When observing such a spectrum it is not obviously clear that these four lines correspond to the same paramagnetic species. However, a closer look into the properties of Au atoms helps to rationalize the appearance of the spectrum. Au consists exclusively of the isotope ^{197}Au having a nuclear spin of $I = 3/2$. The unpaired electron couples to the nuclear spin of the Au atom. This is called hyperfine interaction. Therefore, it is expected that the Zeeman line splits into four peaks due to the interaction of the unpaired electron with the 4 different nuclear spin states of Au. Note that a statistically picked Au atom within the ensemble will have a certain nuclear spin state and give rise to one of the four lines observed in the spectrum. Because of the equipartition of the nuclear spin states even at 30 K, all four nuclear spin states are populated equally and thus the Boltzmann weight of each line is identical for an ensemble of spins as observed here. A double integration of the spectrum reveals that within experimental error the four lines have the same intensity despite the fact that the observed signal amplitudes are different. The latter is due to differences in line width observed for the different lines.

The hyperfine interaction plays a pivotal role for the analysis of EPR spectra of many catalytically important systems, because it often allows extracting valuable information on the electronic structure as well as on the environment of the paramagnetic centres. From a qualitative point of view the preceding discussion seems to be sufficient to understand the appearance of the EPR spectrum of Au atoms. However, additional experiments at different angles between the surface and the magnetic field summarized in the lower diagram of Fig. 1a reveal a significant dependence of the resonance positions on the orientation of the magnetic field. A more detailed description is required to understand this behaviour, but also to extract information on the structural and electronic properties of the species. The framework to achieve this goal is the description of the system by a so-called spin Hamiltonian (eqn (1)), which – for the current discussion – consists of two terms reflecting the electron Zeeman and hyperfine interactions.

$$\hat{H} = \mu_B \vec{S} \boldsymbol{g} \vec{B} + \vec{S} \boldsymbol{A} \vec{I} \tag{1}$$

μ_B denotes the Bohr magneton, $\vec{B}$, $\vec{S}$ and $\vec{I}$ are the vectors of magnetic field, electron spin and nuclear spin, respectively. The dependence of the resonance position on the angle between the surface and the magnetic field indicates anisotropic interactions, which imply that scalar values of g and A will not be sufficient to describe this system. Such anisotropic interactions are well known in physics and can be described by means of tensors. Eqn (1) gives the Hamiltonian for paramagnetic centres characterized by Zeeman and Hyperfine interaction. The corresponding $\boldsymbol{g}$ and $\boldsymbol{A}$ tensors have the form of 3×3 matrices as exemplarily shown in eqn (2) for the g matrix.

$$\boldsymbol{g} = \begin{bmatrix} g_{xx} & g_{xy} & g_{xz} \\ g_{yx} & g_{yy} & g_{yz} \\ g_{zx} & g_{zy} & g_{zz} \end{bmatrix} \tag{2}$$

View Online

Table 1 Correlation of point group symmetry and symmetry properties of EPR parameters.

Symmetry of EPR parameters	Relationship between *g*- and *A*-matrix elements	Relationship between the axis of the coupling matrices	Point group symmetry of the system
Isotropic	$g_{11} = g_{22} = g_{33}$ $A_{11} = A_{22} = A_{33}$	All axis coincident	O, O_h, T, T_d, T_h
Axial	$g_{11} = g_{22} \neq g_{33}$ $A_{11} = A_{22} \neq A_{33}$	All axis coincident	$D_{\infty h}$, $C_{\infty v}$, D_{6h}, D_6, C_{6v}, D_{4h}, D_4, C_{4v}, D_{3h}, D_{3d}, D_3, C_{3v}, D_{2d}
Rhombic	$g_{11} \neq g_{22} \neq g_{33}$ $A_{11} \neq A_{22} \neq A_{33}$	All axis coincident	C_{2v}, D_2, D_{2h}
Axial non collinear	$g_{11} = g_{22} \neq g_{33}$ $A_{11} = A_{22} \neq A_{33}$	g_{zz} collinear with A_{zz}	C_3, C_{3h}, C_4, C_{4h}, S_4, C_6, C_{6h}, S_6
Monoclinic	$g_{11} \neq g_{22} \neq g_{33}$ $A_{11} \neq A_{22} \neq A_{33}$	One axis of *g* and *A* collinear	C_2, C_{2h}, C_S
Triclinic	$g_{11} \neq g_{22} \neq g_{33}$ $A_{11} \neq A_{22} \neq A_{33}$	All axis non coincident	C_1, C_i

Published on 05 February 2015 on http://pubs.rsc.org | doi:10.1039/9781782622697-00001
Downloaded on .

The *g* and *A* matrices are symmetric and can thus be diagonalized, which means that all off-diagonal elements vanish. The components g_{xx}, g_{yy}, g_{zz} and A_{xx}, A_{yy}, A_{zz} (or g_{11}, g_{22}, g_{33} and A_{11}, A_{22}, A_{33}) of the diagonal matrices are also called principal components. It is important to note that these principal components correspond to a well-defined Cartesian coordinate system within the local framework of the paramagnetic centre. In general, symmetry is a powerful tool to predict the properties of the coupling matrices. Table 1 summarizes the relationship between *g* and *A* matrix components and their relative orientation with the point group symmetry of a paramagnetic site.[30]

Information on the system can be deduced from the experiments by simulations, which allow extracting the principal components of the *g*- and *A*-matrices. There are different levels of sophistication depending on the size of the hyperfine interaction with respect to the Zeeman interaction. For systems with rather large hyperfine interaction such as Au atoms discussed here, it is not sufficient to consider the hyperfine interaction as a perturbation on the Zeeman interaction. This implies that the eigenvalue problem associated with the Hamiltonian of eqn (1) has to be solved. This is *e.g.* implemented in the freely available program package easy spin, a very powerful toolbox to simulate EPR spectra.[31] Fits of the angular dependent EPR spectra using this program package were made and the results are shown as grey traces in the upper and lower plot of Fig. 1a. Which assumptions have been made to simulate the spectrum? First, it is important to realize that the spectrum contains four lines. Given the fact that the resonance positions are a function of the orientation of the centre with respect to the external magnetic field, all centres contributing to an individual EPR line behave similarly. Therefore, within one spectrum the principal components as well as the orientation of the coupling matrices are very similar for all centres. This is the typical scenario for a single crystal containing one well-defined paramagnetic species.

Table 2 Principle components of the *g*- and *A*-matrix for Au atoms on MgO.[29]

$\boldsymbol{g}_{\perp} = g_{xx} = g_{yy}$	2.0652
$\boldsymbol{g}_{\parallel} = g_{zz}$	1.9904
$\boldsymbol{A}_{\perp} = A_{xx} = A_{yy}$	1402 MHz
$\boldsymbol{A}_{\parallel} = A_{zz}$	1410 MHz

Published on 05 February 2015 on http://pubs.rsc.org | doi:10.1039/9781782622697-00001
Downloaded on .

The principle components of the *g* and the *A* matrix extracted from the fits are shown in Table 2. In addition to the values one gets the orientation of the matrices with respect to the surface. It is clear that the latter information can only be extracted for macroscopically ordered systems such as planar single crystalline surfaces used here. It is found that one of the principal components is oriented perpendicular to the surface while the other two components lying in the surface plane are degenerated, which was shown by an independent experiment with an appropriately rotated crystal (not shown). The knowledge about the orientation of the coupling matrices gives the possibility to infer that the Au atoms contributing to the spectrum are located on the islands of the MgO(001) surface, because adsorption of Au atoms at structural defects such as steps, corners, or kinks would cause a tilt of the orientation of the magnetic interaction matrices away from the surface normal and in turn a significant change of the angular dependence of the spectra. It does not mean that Au atoms do not adsorb to step edges or corner sites, which they do as seen from the STM image (Fig. 1b) taken at 4 K on a single crystalline MgO(001) film, but these atoms do not contribute to the observed EPR signal, because of their comparably low abundance.

The behaviour of the signal amplitude is due to small differences in the hyperfine coupling constant within the ensemble. The interested reader is referred to the literature for details.[29]

The situation on a single crystalline surface differs of course from that in a powder. Assuming the same adsorption behaviour, the EPR spectrum of such a powder material is considerably different, because the sample contains all orientations at ones, which were investigated separately in the single crystal case. Hence, the spectrum is an appropriately weighted superposition of the spectra for each orientation. Fig. 1c shows a simulation of the expected line shape neglecting the dependence of the hyperfine coupling constant on the adsorption sites. It is seen that each of the hyperfine lines from Fig. 1a is now a pattern determined by the *g*-anisotropy, where the low field maximum corresponds to $g_{\perp}$ and the high field minimum to $g_{\parallel}$ as indicated in Fig. 1c. In this particular case the situation is rather simple, because the hyperfine interaction is almost isotropic and large. Thus, the effect of the *g*-matrix anisotropy on the individual hyperfine lines is clearly visible. It is obvious that the spectrum interpretation of a powder sample can be much more complicated when both the *g*- and *A*-matrix are anisotropic and the resulting lines overlap. For a complex EPR spectrum some experience is required to deduce an appropriate spin Hamiltonian together with the matrix elements of the coupling matrices from a given line shape. In general it

requires some knowledge about the system and possible paramagnetic centres in the first place.

3.2 Physical interpretation of *g*- and *A*-matrix components: a primer

One of the core results of the spectral analysis was the determination of the characteristic coupling parameters namely the anisotropic hyperfine and the Zeeman interaction. However, a very important question remains: What additional insight can be obtained from the values of the *g* and *A* matrices? The discussion of this crucial aspect is in general rather involved, but valuable insight can often be achieved based on a qualitative or semi-quantitative discussion of the expected electronic structure of the site under consideration, *e.g.* an analysis of the crystal field of a transition metal ion. Significant progress in this respect has been made in recent years by computational approaches mostly based on DFT methodologies, which are now capable to calculate *g* and *A* matrix components with sufficient precision for meaningful comparisons (see *e.g.* ref. 32–38). This has advanced the understanding of paramagnetic centres tremendously. Even though the following examples will be taken from the field of paramagnetic centres on solid surfaces, the impact is perhaps even more severe in the field of molecular or biological systems.

Information on the electronic properties of the system at hand is encoded in both the *g*- and the *A*-matrix. Conceptually, it is perhaps easier to start with the discussion using the hyperfine interaction. As mentioned above the hyperfine interaction is a symmetric (3×3) matrix, which can be diagonalized. This diagonal matrix has in general a trace, but it is possible to decompose the matrix into two parts: an isotropic, scalar part (a_{iso}) and an anisotropic dipolar part ($\boldsymbol{T}$), which is a traceless (3×3) matrix. Mathematically this can be written as follows:

$$\boldsymbol{A} = \begin{pmatrix} A_x & 0 & 0 \\ 0 & A_y & 0 \\ 0 & 0 & A_z \end{pmatrix} = a_{iso} \begin{pmatrix} 1 & 0 & 0 \\ 0 & 1 & 0 \\ 0 & 0 & 1 \end{pmatrix} + \begin{pmatrix} T_1 & 0 & 0 \\ 0 & T_2 & 0 \\ 0 & 0 & T_3 \end{pmatrix} \quad (3)$$

The reason for this decomposition is that these two parts of the hyperfine interaction can be associated with different physical effects. The isotropic hyperfine coupling constant is also known as the Fermi contract term and is due to the finite probability to find the electron at the nucleus. For Au atoms on MgO a large isotropic hyperfine coupling constant is expected, because the spin is predominately of s character (unpaired electron in the 6s orbital) and should thus have an appreciable density at the nucleus. While this is qualitatively expected, it is interesting to note that the isotropic hyperfine coupling constant of the adsorbed Au atoms is more than 50% smaller than the corresponding value measured for Au atoms in a rare gas matrix.[39] What is the reason for the reduced s electron spin density on the MgO surface? On the one hand the spin density itself could be reduced *e.g.* by partial charging of the Au atoms on the surface. On the other hand it is possible that the s character of the spin density is reduced. These two effects cannot easily be disentangled based on the experimental results alone. However, theoretical calculations can help to answer this question. Proper density

Published on 05 February 2015 on http://pubs.rsc.org | doi:10.1039/9781782622697-00001
Downloaded on .

Published on 05 February 2015 on http://pubs.rsc.org | doi:10.1039/9781782622697-00001
Downloaded on .

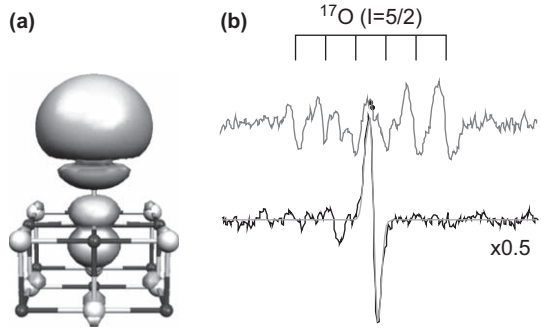

Fig. 2 (a) Calculated spin density of Au atoms adsorbed on oxygen ions of a MgO(001) surface. (b) EPR signal of the most intense line from Fig. 1a (bottom trace) and spectrum found after growth of a ^{17}O enriched MgO(001) film (top trace).

functional calculations revealed that the charge transfer from or onto the Au atoms is small. One the other hand the shape of the spin density as shown in Fig. 2a is no longer spherical as expected for s orbitals, but the spin density and thus the wave function is polarized away from the surface as a result of the Pauli repulsion with the oxygen anions of the surface. In a simple orbital picture this implies that the corresponding wave function contains components with higher angular momentum l (p or d orbitals), which reduces the s contribution and, thus, the isotropic hyperfine interaction. From an energetic point of view this implies that the Au 6s orbital is destabilized due to the Pauli repulsion with the lattice oxygen ions of the MgO. This effect is not restricted to coinage metals on MgO, but has been seen before *e.g.* for alkali metals on MgO or coinage metals on alkali chloride surfaces.[40–42]

Hyperfine interaction extends also beyond the atom or atoms where the spin density is mainly localized. The hyperfine interaction found on more distant atoms is often called superhyperfine interaction (shf). To exemplify the kind of information, which can be accessed, Fig. 2b shows the largest EPR line of Au atoms observed for MgO grown with conventional oxygen (bottom trace), and the spectrum measured after growing the MgO(100) surface with $^{17}O_2$ ($I = 5/2$; 90% enrichment) (top trace).[29] The single line is split into six lines and a small signal at the original position. The latter is due to Au atoms interacting only with ^{16}O in the film. The observed intensity is about 10% of the original one. Given an isotopic enrichment of 90%, this indicates significant coupling of the Au atom to one oxygen ion only. This is in line with the sextet of lines, which can be readily understood by a coupling of the unpaired electron of the Au atom to one ^{17}O in the film. Hence all adsorption sites having more than one equivalent oxygen neighbour such as the Mg cation site can be excluded. In particular, it is perfectly consistent with the preferred adsorption site according to theory being Au adsorbed on top of the oxygen anions of the film.[43,44]

Apart from the hyperfine interaction also the *g*-matrix contains valuable information. The extraction of this information is intimately linked to the electronic structure of the system at hand. For transition metal

Published on 05 February 2015 on http://pubs.rsc.org | doi:10.1039/9781782622697-00001
Downloaded on .

ions being a prominent class of paramagnetic centres in catalytic systems, crystal field theory is the basis of the qualitative and semi-quantitative discussions. The various situations found for transition metal ions have been investigated early on and there are excellent books and reviews summarizing their properties (*e.g.* ref. 30, 45 and 46). Here the information encoded in the *g*-matrix components will be exemplified using $O_2^{\bullet-}$ radicals on MgO(001). Adsorption of molecular oxygen at 30 K on a 4 ML thick MgO(001) film grown on a Mo(001) single crystal leads to the spontaneous formation of $O_2^{\bullet-}$ radicals characterized by the angular dependent EPR spectra shown in Fig. 3a.[47]

The analysis of the presented spectra together with spectra taken at a different azimuthal orientation of the (001) surface with respect to the magnetic field (not shown) reveal an orientation of principal components of the $O_2^{\bullet-}$ *g* matrix along the surface normal and the [110] equivalent directions within the (001) surface (the third one is orthogonal on the other two). This proves that the radical is adsorbed on the terraces of the MgO(001) islands and aligned with [110] equivalent directions (Fig. 3b). This is in perfect agreement with theoretical predictions for the adsorption site.[48,49] More important for the present discussion are the values of the *g*-matrix elements, in particular the g_{zz} component. For this discussion $O_2^{\bullet-}$ radicals on the thin films are compared to $O_2^{\bullet-}$ centres on MgO powder. The radicals do not form spontaneously on the stoichiometric surface of the powders, but extra electrons are required as introduced *e.g.* by alkali metal atom doping.[50–53] A detailed analysis of the powder data in comparison with theoretical calculations revealed that the g_{zz} component of the matrix strongly depends on the adsorption site. In particular, radicals adsorbed on morphological defects such as edges

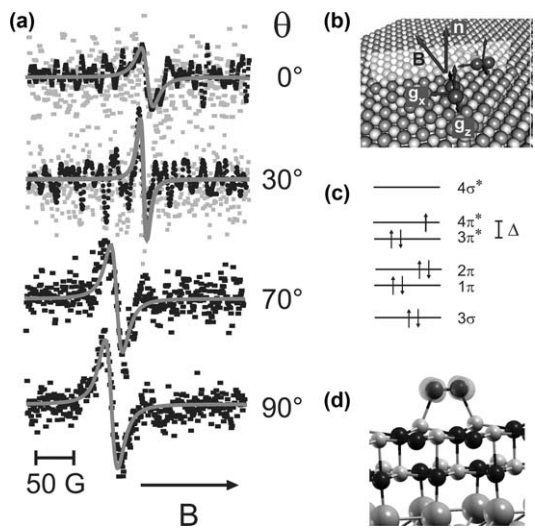

Fig. 3 (a) Angular dependent EPR spectra of $O_2^{\bullet-}$ radicals spontaneously formed on 4 ML thick stoichiometric MgO(001) film on Mo(001). (b) Schematics of the experimental geometry. (c) Schematic MO diagram of an $O_2^{\bullet-}$ radical. (d) Binding geometry as calculated theoretically.

View Online

Table 3 Measured g matrix components for $O_2^{\bullet-}$ radicals adsorbed on the surface of thin MgO(001)/Mo(001) films and MgO powders.

	Site	g_{xx}	g_{yy}	g_{zz}
MgO/Mo(001) exp.[47]	Terrace	2.002	2.012	2.072
MgO powders exp.[56]	Terrace	2.002	2.008	2.091
MgO powders exp.[57]	Edge	2.002	2.008	2.077

Published on 05 February 2015 on http://pubs.rsc.org | doi:10.1039/9781782622697-00001
Downloaded on .

or corners show a significant reduction of the g_{zz} component as compared to the regular terraces site (Table 3). The reason is that for such a 13 electron radical the g_{zz} component of the molecule can be given to first order by the following expression:[54]

$$g_{zz} = g_e + 2[\lambda^2/(\lambda^2 + \Delta^2)]^{1/2} \quad (4)$$

in which λ is the spin orbit coupling constant and Δ is the energy difference between the singly and the doubly occupied π^* orbitals as depicted in Fig. 3c. The equation also reminds on the fact that the origin for the deviation of the g matrix components from the free electron values is due to spin orbit interaction. The reduction of the g_{zz} component with a reduction of the local coordination of the adsorption site on an ionic crystal is directly associated with an increase of the local electric field at the adsorption site. An increased electric field leads to an increased splitting between the π^* orbitals of the $O_2^{\bullet-}$ radical and hence to an increase of Δ. In turn, the g_{zz} component will be found closer to the value of the free electron, which is the explanation for the experimental observation made on powders. What is the reason for the reduced g_{zz} values measured for $O_2^{\bullet-}$ radicals on terraces of the thin film compared to terrace sites on the MgO powders? The explanation is intimately related to the question of the stability of the $O_2^{\bullet-}$ radicals on the thin MgO film. Theory predicts that the electron transfer from the metal substrate (Mo(001)) through the MgO film onto the oxygen molecule is stabilized by a so-called polaronic distortion of the MgO lattice, an effect considered important not only for molecules but also for metal adsorbates with high electron affinity such as Au.[48,49,55] This means that the ions underneath the $O_2^{\bullet-}$ radical are pulled out of their regular lattice positions as indicated in Fig. 3d which, according to theory, is the important mechanism to stabilize the charge transfer state. The polaronic distortion gives rise to an increase of the electric field encountered by the oxygen molecule on the surface and thus a reduction of the g_{zz} component of the g matrix. EPR spectroscopy provides the first experimental evidence for the existence of the polaronic distortion for such a system, which is difficult to observe experimentally for such systems.

3.3 Impact of rotational dynamics on cw-EPR spectra

The paramagnetic Au atoms discussed above were considered as static entities and at a measurement temperature of 30 K this assumption is justified. However, catalytic systems are often investigated at elevated temperatures or molecular catalysts are studied in the liquid phase. For such systems the assumption that the paramagnetic species are static